

Elementary scaling laws for sizing up and down Hall effect thrusters: Impact of simplifying assumptions.

IEPC paper 2009-077

*Presented at the 31st International Electric Propulsion Conference,
University of Michigan ◊ Ann Arbor, Michigan ◊ USA
September 20 - 24, 2009*

K. Dannenmayer¹, S. Mazouffre²

*Institut de Combustion, Aérothermique, Réactivité et Environnement,
CNRS, 1C avenue de la Recherche Scientifique, 45071 Orléans, France.*

Abstract – Various sizing methodologies are currently available to get a first estimate of the required Hall effect thruster dimensions for a given input power and a corresponding thrust and specific impulse level. In this work, a semi-empirical approach to compute the three characteristic thruster dimensions, i.e. the channel length, the channel width and the channel mean diameter as well as the magnetic field strength, is introduced. The determination of the scaling laws is based on analytical relationships deduced from the physical mechanisms that govern the properties of a Hall thruster discharge. A set of simplifying assumptions naturally specifies the validity domain of the relationships. The existence of a critical propellant atom density inside the channel, which warrants a high-efficiency thruster operation, is revealed and commented. This “density constraint” leads to a mere linear relation between the channel diameter and width, which is then used to refine the set of scaling laws. The proportionality coefficients of the scaling laws are assessed by way of a vast database that comprises 33 single-stage Hall effect thrusters covering a power range from 10 W up to 50 kW. The sizing method is employed to access the geometry and the operating parameters for a 20 kW-class as well as a 100 kW-class Hall thruster. Results obtained with two different series of simplifying assumptions are compared. The first set forms a very restrictive frame. The second set offers a more realistic description of the physics at work as the electron temperature, the energy losses and multiply-charged ion species are taken into account.

Nomenclature

A	channel cross section; area
\mathbf{B}	magnetic field
C_{B_1}, C_{B_2}	proportionality coefficient for the magnetic field
C_I	proportionality coefficient for the discharge current
$C_{I_{sp}}$	proportionality coefficient for the specific impulse
C_P	proportionality coefficient for the power
C_{T_1}, C_{T_2}	proportionality coefficient for the thrust
C^*	proportionality coefficient under low assumptions
d, d_{ext}, d_{int}	mean, external and internal channel diameter
e	elementary charge
\mathbf{E}	electric field
f_{2+}	fraction of doubly-charged ions
g_0	Earth standard gravity

¹Ph.D. student, Electric Propulsion team, kathe.dannenmayer@cnrs-orleans.fr

²Research Scientist, Electric Propulsion team leader, stephane.mazouffre@cnrs-orleans.fr

h	channel width
$I, I_d, I_{\text{Hall}}, I_i$	current, discharge current, Hall current, ion current
I_{sp}	specific impulse
j_{Hall}	Hall current density
j_e, j_i	electron, ion current density
k	index-number
k_B	Boltzmann constant
L	channel length
m_e, m_n, m_i	electron mass, propellant atom mass, ion mass
\dot{m}_n, \dot{m}_i	propellant mass flow rate through the anode, ion mass flow rate
n_e, n_i, n_n	electron, ion and atom number density
$n_{n,c}$	critical atom density
P, P_{in}	discharge electrical power, overall input power
P_{loss}	power losses due to plasma-wall interactions
r, R	inner, respectively outer, channel radius
r_{Le}, r_{Li}	electron and ion Larmor radius
S	surface
T	thrust
T_e, T_n	electron temperature, atom temperature
U_d	discharge voltage
v_e, v_n	thermal speed of electrons and atoms
v_{ex}	propellant exhaust velocity
v_i	ion flow velocity
V	volume
Z	atomic number
α	propellant conversion efficiency
Δ	voltage losses
η_T, η_A	thrust efficiency, anode efficiency
γ, γ'	correction factors for the presence of multiply-charged ions
λ_i, λ_{ee}	ionization and electron-electron collision mean free path
μ_e	electron mobility
ν_{ce}	electron gyrofrequency
ν_{en}	electron-atom collision frequency
ν_i	ionization frequency
π	mathematical constant π
ξ	scaling index variable
σ_i, σ_{ee}	cross-section for ionization and electron-electron impact
σ_{en}	electron-atom momentum exchange cross-section
τ_{ce}	gyroperiod
τ_{en}	electron-atom collisional time
θ_d	beam divergence correction term

I. Introduction

Electric propulsion is at present a well-established technology for space applications¹. Among all proposed electric propulsive devices such as arcjet, magnetoplasmadynamic thruster, gridded ion engine and Hall Effect Thruster (HET), the latter is currently recognized as an attractive propulsion means for long duration missions and for maneuvers that require a large velocity increment. Hall effect thrusters are advanced propulsion devices that use an electric discharge with magnetized electrons to ionize and accelerate a propellant gas^{2,3}. Due to interesting features in terms of propellant ejection speed, efficiency, thrust-to-power ratio and lifetime, HETs are now employed for missions like geosynchronous satellite attitude correction and station keeping. Moreover, HETs appear as good candidates to be used as the primary propulsion engine for space probes during interplanetary journeys, as demonstrated by the successful SMART-1 Moon flyby solar-powered mission of the European Space Agency⁴.

A schematic of a Hall effect thruster is depicted in Fig. 1. The basic physics of a HET implies a magnetic barrier and a low pressure DC discharge generated between an external hollow cathode and an anode in such a way that a crossed electric and magnetic field discharge is created^{2,3,5,6}. The anode,

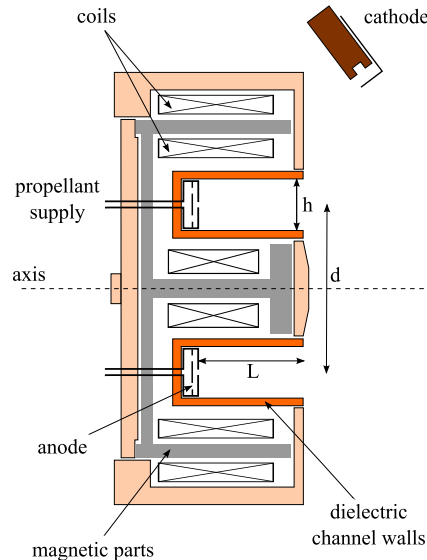


Fig. 1: Cross-section view of a Hall effect thruster showing the main components. The three characteristic dimensions L , h and d are also indicated.

which also serves as gas injector, is located at the upstream end of a coaxial annular dielectric channel that confines the discharge. Xenon is generally used as a propellant gas for its specific properties in terms of high atomic mass and low ionization energy. A set of solenoids provides a radially directed magnetic field \mathbf{B} of which the strength is maximum in the vicinity of the channel exhaust. The magnetic field is chosen strong enough to make the electron Larmor radius much smaller than the discharge chamber length, but weak enough not to affect ion trajectories. The electric potential drop is mostly concentrated in the final section of the channel owing to the low electron axial mobility in this restricted area. The corresponding induced local axial electric field \mathbf{E} has two main effects. First, it drives a high electron azimuthal drift – the Hall current – that is responsible for the efficient ionization of the supplied gas. Second, it accelerates ions out of the channel, which generates thrust. The ion beam is neutralized by a fraction of electrons emitted from the hollow cathode. When operating near 1.5 kW, a HET ejects ions at 20 km s^{-1} and generates 100 mN of thrust with an overall efficiency of about 50 %.

Space agencies together with platform manufacturers and users nowadays envisage new fields of application for electric propulsion systems that require low and high power devices. Low power Hall thrusters ($\sim 100 \text{ W}$) are well suited for drag compensation of observation satellites that operate on a low-altitude orbit in the Earth atmosphere as well as for trajectory correction of small platforms and microsatellite constellations. The use of high power ($\sim 5 \text{ kW}$) Hall thrusters for orbit raising and orbit topping maneuvers of communication satellites would offer significant benefits in terms of launch mass, payload mass and operational life. In addition, journeys towards far-off planets and asteroids with large and heavy robotic probes and Moon and Mars cargo missions necessitate to build thrusters with an input power in the range of 10-100 kW. In view of the projects demand, it appears necessary to expand the operating envelope of existing Hall effect thruster technology to achieve the required performance level. A non-trivial question then arises: How to extrapolate the design and architecture of currently existing Hall thrusters towards different scales and different operating conditions? In other words, what are the scaling laws that connect Hall effect thruster characteristic dimensions with operating parameters like discharge voltage, propellant mass flow rate and magnetic field strength and performances in terms of thrust, specific impulse and overall efficiency?

II. Overview of previous studies and aim of the work

Scaling laws that govern the physical properties, the accelerating ability as well as propellant and energy consumption of Hall thrusters have been extensively investigated by numerous authors since the period of development of Hall thrusters in the 70's. In spite of decades of research on this subject, the assessment of scaling laws is still a topic of great interest as various methodologies and results exist. Therefore, before describing the approach associated with this study as well as its outcomes, it is worth briefly reviewing works carried out on this topic during the past few years and available in the open literature.

According to the pioneer works of the Russian physicist A. Morozov⁵, in order to derive scaling laws, it is necessary to find a similarity criterion, or a set of criteria, that warrant the underlying physical processes to stay unchanged whatever the thruster. This principle states that the properties of thrusters with a different geometry are linked by way of scaling laws only if a sufficiently large number of dimensionless similarity criteria coincide. The complete set of similarity criteria has not yet been found, however, all works show that the *Melikov-Morozov criterion* has a strong impact on HET behavior and characteristics and it must always be taken into account. This criterion indicates that $\lambda_i \ll L$. In addition to similarity criteria, the investigation of scaling laws for Hall thrusters necessitates to account for simplifying assumptions, e.g. a frozen electron temperature, and constraints like a high efficiency and a reasonable channel wall temperature.

V. Zhurin and co-workers proposed a size scaling method which is limited to the effects of changing either the channel width h or the channel mean diameter d ². One assumption is that the channel mean diameter is much larger than the channel width, so that variation of parameters in the radial direction are negligible. Furthermore, they considered a fixed discharge voltage. In order to obtain similar performances for two different thruster configurations, authors showed that the ratio of r_L , λ and L to h must stay the same for the two configurations. Using these criteria and a set of assumptions they demonstrate that the magnetic field strength is inversely proportional to the channel width, $B \propto 1/h$, whereas the discharge current and the propellant mass flow rate are inversely proportional to the channel mean diameter, $I_d \propto 1/d$ and $\dot{m} \propto 1/d$.

It was demonstrated by V. Kim⁶ that to reach a high level of efficiency it is not only necessary to ionize and accelerate ions but to accelerate them into the proper direction, hence the need for an optimized magnetic field topology. In short, for a HET with an optimized magnetic field map, there is a relationship between the acceleration layer length L_a and the magnetic layer characteristic size L_B and between L_a and h . The use of these similarity criteria, which include the magnetic field structure, permits to simplify the development of new Hall thrusters models. V. Kim and co-workers also emphasize the fact that in the case of a traditional HET design, the ratio of the ionization mean free path to the channel length must stay constant (*Melikov-Morozov criterion*)⁷. Moreover they give additional criteria about the geometry of thruster elements, i.e. L and d are both proportional to h , that are equivalent to the ones given by V. Zhurin. There are two immediate consequences. First, the propellant mass flow density and the power density rise when the thruster size decreases, assuming a constant discharge voltage. Second, as the magnetic field strength is connected with the characteristic dimensions, notably the channel width, and with the operation mode, the magnetic field magnitude must rise when the size reduces in order to keep comparable conditions.

The method presented by J. Ashkenazy et al. concerns low power scaling and it is based on the idea of a sufficient propellant utilization⁸. They show by means of a simplified analysis that a straightforward approach for scaling down the channel size results in a rise of power losses and a reduced overall thruster efficiency. To avoid these effects, the acceleration region has to be scaled down along with the channel width and the magnetic field strength must be increased in proportion to $1/h$. They also describe an alternative view that consists in extending the channel length.

M. Martinez-Sanchez et al. developed an approach for low-power Hall effect thrusters that includes the use of reference points⁹. The goal is to achieve a reduction in the thrusters length scale while preserving both the thrust efficiency and the specific impulse. The main result of their study is that the propellant mass flow rate and the applied power scale as the channel length, $\dot{m} \propto L$ and $P \propto L$, whereas the magnetic field strength is in inverse proportion to the latter, $B \propto 1/L$. This scaling method allows to calculate the channel size and the performances of a small thruster with a given input power provided that a well-known thruster is utilized as a reference.

Daren Yu and his team suggested an improvement of the existing scaling theory by introducing a scaling index variable¹⁰. They assume that the electron temperature and the discharge voltage are constant, that the ratio λ_i/L is constant and that the geometric similarity is given by $r/R=\text{constant}$ and $R^{2-\xi}/L=\text{constant}$, where R and r are the channel outer respectively inner radius and ξ represents a scaling index variable. They show by way of a comparison of experimental data with numerical outcomes for different values of ξ , that results obtained from their scaling theory agree well with the experimental data for $\xi=2$. Therefore they deduce that the number density n is constant, whereas the mass flow rate \dot{m} , the input power P , the thrust T and the discharge current I_d are proportional to the square of the outer channel radius R .

Finally, the team led by M. Andrenucci advised to employ an analytical model coupled to an existing Hall thruster database¹¹. This scaling methodology aims to provide design options for high power

thrusters. The idea is to create a vector of fundamental parameters defining the thruster geometry and its performances. This vector is composed of three geometric parameters (L , h and d), the gas number density in the injection plane and the applied discharge voltage U_d . A scaling matrix derived from the Hall thruster physical principles allows to obtain a new thruster characteristics on the basis of a reference thruster.

In a recent article¹², we put forward an original way to extrapolate Hall thruster geometry and magnetic field strength towards both the low and high power ranges. The approach is based on the combination of a set of scaling laws that are extracted from fundamental equations along with a vast body of existing data. Strong assumptions are made to define the working frame: Among others, quantities are steady and homogeneous in the plasma, the applied potential energy is fully converted into axial kinetic energy and all xenon ions are singly-charged. Our study indicates: $P \propto hd/L$, $T \propto hd/L$ and $B \propto 1/hd$. Besides, realistic constraints on the performance level and on the thermal load are added in order to limit the set of possible L , h and d characteristic lengths when sizing a thruster for a given input power or thrust level.

In this contribution, the scaling laws and the sizing methodology previously worked out are refined by taking into account an atom density constraint inside the channel, which leads to the fact that the channel mean diameter d is proportional to the channel width h ($d \propto h$). Furthermore, we study the effect of reducing the number of simplifying assumptions. A new set of scaling laws is then given when considering the evolution of the electron temperature T_e , the voltage losses Δ and the fraction of doubly-charged ions f_{2+} as a function of the discharge voltage U_d as well as the ion beam divergence. The two sets of scaling laws obtained under high and low assumptions are subsequently used to determine the geometry and the operating parameters of two high-power Hall thrusters, namely a 20 kW-class and a 100 kW-class thruster.

III. Set of governing relations and scaling

A Ionization and plasma containment

The geometry of a Hall effect thruster is defined by three characteristic dimensions, namely: the discharge channel length L , the channel mean diameter $d = \frac{1}{2}(d_{ext} + d_{int})$ and the channel width h . For the sake of clarity, the three sizes are shown in Fig. 1. As we will see, the thruster geometry depends upon a set of operating parameters such as the discharge voltage U_d and the propellant mass flow rate \dot{m} , as well as upon the magnetic field strength B .

A necessary first step in order to determine scaling laws for Hall thrusters does consist in finding some critical parameters as well as in defining similarity criteria based on the current knowledge and understanding of the physics of Hall thrusters. Therefore, the two processes at the origin of thrust generation, i.e. propellant ionization and plasma confinement, must be considered and critically examined. In the remainder of this paragraph, all quantities are assumed to be steady in time and homogeneous in space in order to permit the derivation of necessary equations.

A.1 Propellant Ionization

The first relationship reflecting the impact of the thruster scale on its performance is the relationship between the discharge channel length L and the ionization mean free path λ_i . To ensure a sufficient ionization of the gas, it is necessary to satisfy the so-called Melikov-Morozov criterion:

$$\lambda_i \ll L. \quad (1)$$

The ionization frequency that originates from electron-atom impacts reads:

$$\nu_i = n_n \langle \sigma_i(v_e) v_e \rangle \approx n_n \sigma_i(T_e) \sqrt{\frac{8k_B T_e}{\pi m_e}}. \quad (2)$$

The ionization length, which corresponds to the mean distance an atom can travel before being ionized, can be formulated as the product $\nu_i v_n$ in a first order approximation. Therefore the Melikov-Morozov criterion can be expressed as:

$$\lambda_i = \frac{v_n(T_n)}{n_n \sigma_i(T_e) v_e(T_e)} \ll L. \quad (3)$$

The atomic gas flows almost randomly inside the discharge chamber. Indeed, in the case of xenon gas, the axial velocity is at most twice larger than the thermal speed at the channel outlet due to consumption of slow atoms in the course of the ionization process. As a consequence, one must also consider the radial motion of atoms for comparison with the ionization mean free path. Ionization of the injected gas is efficient within a Hall thruster provided that:

$$\lambda_i \ll h. \quad (4)$$

A.2 Electron and ion containment

The magnetic field strength in a Hall effect thruster is such that electrons are magnetized and ions are not, or at least weakly, magnetized. The following criterion must then be fulfilled⁶:

$$r_{Le} \ll L \ll r_{Li}. \quad (5)$$

The definition of the electron Larmor radius is:

$$r_{Le} = \frac{m_e v_e(T_e)}{eB}. \quad (6)$$

Using the fact that the ratio of r_{Le} to L must remain constant, the following relationship can be established:

$$B \propto \frac{m_e v_e(T_e)}{eL}. \quad (7)$$

The relation 7 between B and L has already been mentioned by M. Martinez-Sanchez⁹. A second constraint for the magnetic field strength can be established due to the fact that the electron gyroperiod τ_{ce} in the magnetic barrier must be much shorter than the time between two consecutive electron-atom collisions τ_{en} :

$$\frac{\tau_{en}}{\tau_{ce}} = \frac{\nu_{ce}}{\nu_{en}} \gg 1, \quad (8)$$

where $\nu_{ce} = eB/m_e$ and $\nu_{en} = n_n \sigma_{en} v_e$ ¹³. This strong point indicates that electrons must be efficiently trapped inside the magnetic field of a Hall thruster in order to produce a high electric field and to favor ionization of the seeded gas. In fact, τ_{en} is so long in a HET that anomalous electron transport perpendicular to the magnetic field lines must be put forwards to correctly explain the observed properties and the magnitude of measured quantities^{2,5,14}. Assuming that the ratio ν_{ce}/ν_{en} must remain constant, Eq. (8) implies:

$$B \propto \frac{m_e}{e} \sigma_{en}(T_n, T_e) v_e(T_e) n_n. \quad (9)$$

Aforementioned equations indicate that B depends upon the gas density n_n in compliance with the fact that plasma containment depends on collision events with neutrals.

A.3 Particle density

As previously mentioned, the value λ_i is linked to the channel length and width. In like manner, the electron-electron impact mean free path λ_{ee} is connected with both L and h . The quantity λ_{ee} reads:

$$\lambda_{ee} = \frac{1}{n_e \sigma_{ee}(T_e)}, \quad (10)$$

where the cross-section σ_{ee} is a function of the Coulomb logarithm¹⁵. As the ratio of λ_{ee} to the thruster channel size must stay unchanged, it becomes obvious that:

$$n_e \propto \frac{1}{L} \quad \text{and} \quad n_e \propto \frac{1}{h}. \quad (11)$$

Assuming that both the electron temperature T_e and the propellant speed v_n are constant and weakly dependent upon the thruster operating conditions and keeping the ratio λ_i/L constant, Eqs. 3 and 4 leads to:

$$n_n \propto \frac{1}{L} \quad \text{and} \quad n_n \propto \frac{1}{h}. \quad (12)$$

The relations 11 and 12 for the electron, respectively the atom, number density are the same than those developed before by e.g. V. Zhurin and M. Martinez-Sanchez^{2,9}. Yet, very often authors solely consider the channel length as a critical size for particle density.

Another relation between n_n and Hall thruster dimensions can be established when considering the propellant mass flow rate passing through the anode. The quantity \dot{m} can be decomposed into the product of several terms:

$$\dot{m}_n = n_n \cdot m_n \cdot v_n \cdot A. \quad (13)$$

The annular channel cross section A is given by:

$$A = \frac{\pi}{4}(d_{ext}^2 - d_{int}^2) = \frac{\pi}{4} \underbrace{(d_{ext} + d_{int})}_{2d} \underbrace{(d_{ext} - d_{int})}_{2h} = \pi h d, \quad (14)$$

We can therefore consider that for a constant atom temperature:

$$n_n \propto \frac{\dot{m}_n}{h d}. \quad (15)$$

This relationship between the atom number density and the thruster dimensions h and d has never been mentioned previously, as authors never considered two sizes at the same time. In order to keep the physical processes at work in a Hall effect thruster unchanged, to warrant a high efficiency and to limit the thermal load as well as the channel wall wear, the number densities of electrons and atoms must stay roughly fixed inside the thruster channel whatever the input power, as we will see in a following paragraph.

Magnetic field

Combining Eqs. 9 and 15, one can find a relationship between the magnetic field strength and the hd product:

$$B \propto \frac{\dot{m}_n \sigma_{en}(T_n, T_e) v_e(T_e)}{v_n(T_n)} \frac{1}{h d}. \quad (16)$$

To the best of our knowledge, the correlation between B and a product of two dimensions has never been mentioned before as solely one characteristic thruster dimension is usually considered by authors.

B Relationship between performances and dimensions

The definition of the thrust T , the specific impulse I_{sp} , the various currents, the thrust efficiency η_T and the anode efficiency η_A can be found in many papers and in most textbooks about electric propulsion (see e.g. references [3] and [16]). Here we use the common definitions in order to determine the relationships between Hall thruster functioning parameters, performances and channel characteristic dimensions.

B.1 Thrust

The thrust is the force supplied by the engine to the spacecraft. It is given by the time rate of change of the momentum since the spacecraft mass varies with time due to propellant consumption:

$$T = \frac{d}{dt}(m_n v_{ex}) = \frac{dm_n}{dt} v_{ex}. \quad (17)$$

In a Hall thruster, ions originate in the ionization of the propellant gas and they are accelerated by an electric field within the plasma. The thrust therefore results from the electrostatic acceleration of the ions:

$$T = \dot{m}_i \bar{v}_i = \alpha \dot{m}_n \bar{v}_i, \quad (18)$$

where the coefficient α stands for the fraction of propellant atoms that are converted into ions, whatever the electric charge. For conventional Hall effect thruster, the typical value of α is around 0.9 with xenon when only singly-charged ions are counted. Notwithstanding the fact that ions are not magnetized in a Hall thruster, the presence of a transverse magnetic field is responsible for a large azimuthal drift current, also called Hall current. Indeed, electrons in the plasma feel an $\mathbf{E} \times \mathbf{B}$ force and they move perpendicular to the electric and magnetic field^{2,3}. The Lorentz force electrons experience is equal to the electrostatic force on the ions, hence:

$$T = \int \int \int_V \mathbf{j}_{Hall} \times \mathbf{B} dV \quad (19)$$

$$= 2\pi r \int \int_S \mathbf{j}_{Hall} \times \mathbf{B} dS \quad (20)$$

$$= \pi d I_{Hall} B. \quad (21)$$

To sum up, in a Hall thruster, the thrust is transferred from the ion flow to the thruster body through the magnetic field.

When analyzing the thrust generation in a Hall thruster, one must take into account the presence of multiply charged ion species, especially doubly and triply-charged ions¹⁷ of which the fraction is significant with xenon. If the beam contains the three types of ions, the ion mass flow rate is then:

$$\dot{m}_i = \frac{m_n}{e} I^+ + \frac{m_n}{2e} I^{2+} + \frac{m_n}{3e} I^{3+}, \quad (22)$$

where the superscript indicates the electrical charge. The thrust can in fact be split into a finite series of elementary terms, each of them corresponding to a given ion species:

$$T = m_n \sum_{k=1}^Z \frac{I^{k+} \bar{v}^{k+}}{k e}, \quad (23)$$

where Z is the atomic number. Using the preceding definition for \dot{m}_i , the thrust corrected for the multiple species and for the ion beam divergence can then be written down in the simple form:

$$T = \gamma \theta_d \dot{m}_i \sqrt{\frac{2e}{m_n}} \sqrt{U_d - \Delta} = \alpha \gamma \theta_d \dot{m}_n \sqrt{\frac{2e}{m_n}} \sqrt{U_d - \Delta}, \quad (24)$$

where γ is the multiply charged ion correction factor and θ_d is the beam divergence correction factor. The two factors are described in detail in reference³. They naturally depend on the thruster operating conditions. The preceding equation is obtained under the assumption that all types of ions are produced at the same location and therefore undergo the same potential drop. In other words, the voltage losses for ions are independent of the charge number. In that case, the mean ion exhaust velocity can be defined as⁵:

$$\bar{v}_i = \sqrt{\frac{2e}{m_i} (U_d - \Delta)}. \quad (25)$$

If one considers solely singly and doubly-charged ions, the multiply-charged ion correction factor γ reads:

$$\gamma = \frac{1 + \frac{I^{2+}}{\sqrt{2} I^+}}{1 + \frac{I^{2+}}{2 I^+}}, \quad \gamma = \frac{1 + \frac{f_{2+}}{\sqrt{2}(1-f_{2+})}}{1 + \frac{f_{2+}}{2(1-f_{2+})}}. \quad (26)$$

Combining Eqs. 15 and 24 yields an expression for the thrust as a function of the channel sizes:

$$T \propto \alpha \gamma \theta_d n_n v_n(T_n) \sqrt{U_d - \Delta} h d. \quad (27)$$

As we have shown previously, the atom density n_n is proportional to the channel length (see Eq. (12)). Therefore, the general relationship between the thrust and Hall thruster characteristic sizes reads:

$$T \propto \alpha \gamma \theta_d v_n(T_n) \frac{1}{L} \sqrt{U_d - \Delta} h d. \quad (28)$$

B.2 Specific impulse

The specific impulse is a way to describe the efficiency of rocket and spacecraft engines. It represents the change in momentum per unit of propellant. Essentially, the higher the specific impulse, the less propellant is required to gain a given amount of momentum. In this regard a propulsion method is more propellant-efficient if the specific impulse is higher. The specific impulse is defined by the following equation:

$$I_{sp} = \frac{T}{\dot{m}_n g_0} \approx \alpha \gamma \theta_d \frac{\bar{v}_i}{g_0}, \quad (29)$$

where g_0 is the standard gravity at Earth's surface. Here, \dot{m} refers to the total gas mass flow rate, that means the anode as well as the cathode gas flow rate. When solely the anode mass flow rate is used, strictly speaking the I_{sp} then corresponds to the anode I_{sp} . According to Eq. (24), the specific impulse is not a function of the thruster sizes:

$$I_{sp} \propto \sqrt{U_d - \Delta}. \quad (30)$$

It is solely proportional to the square root of the discharge voltage. Note that for a parallel beam of singly-charged ion species under the condition of full ionization of the supplied propellant, the specific impulse is simply given by the ratio \bar{v}_i/g_0 . This expression is often found in books and articles.

B.3 Electrical power and efficiency

The discharge current is the sum of two components, namely the ion current in the beam and the electron current flowing across the channel outlet: $I_d = I_i + I_e$. Neglecting the electronic part, which is a small fraction of the ionic part (typically 10-20%), one can write:

$$I_d \approx I_i = \sum_{k=1}^Z I^{k+}. \quad (31)$$

The discharge current can easily be expressed in terms of propellant mass flow rate:

$$I_d \approx \frac{e}{m_n} \gamma' \dot{m}_i = \frac{e}{m_n} \gamma' \alpha \dot{m}_n \quad (32)$$

If again solely singly and doubly-charged ions are taken into account, the correction factor γ' is given by:

$$\gamma' = \frac{1 + \frac{I^{2+}}{I^+}}{1 + \frac{I^{2+}}{2I^+}}, \quad \gamma' = \frac{1 + \frac{f_{2+}}{1-f_{2+}}}{1 + \frac{f_{2+}}{2(1-f_{2+})}}. \quad (33)$$

Substituting Eq. (13) into previous equation gives:

$$I_d \approx \pi e \gamma' \alpha n_n v_n(T_n) h d. \quad (34)$$

Finally, from the relation between the gas density and the channel sizes, one finds:

$$I_d \propto \gamma' \alpha v_n(T_n) \frac{h d}{L}. \quad (35)$$

As a direct consequence, the input electrical discharge power is:

$$P = U_d I_d \quad (36)$$

$$\propto \gamma' \alpha v_n(T_n) \frac{h d}{L} U_d. \quad (37)$$

The total efficiency, or thrust efficiency, of a Hall thruster is defined as the mechanical power (or jet power) to the overall electrical power ratio³. It reads:

$$\eta_T = \frac{T^2}{2\dot{m}P_{in}}. \quad (38)$$

The mass flow rate \dot{m} accounts for both the anode and the cathode gas flow rate. The total power P_{in} comprises the discharge power P as well as the power dissipated into the coils and for cathode heating. As the last two quantities are much below the discharge power, the thrust efficiency is often given by:

$$\eta_T = \frac{T^2}{2\dot{m}U_d I_d}. \quad (39)$$

In this work, only the gas flowing through the injector is considered. The thrust is then expressed as the anode efficiency:

$$\eta_a = \frac{T^2}{2\dot{m}_n U_d I_d}. \quad (40)$$

Using the set of available equations for all terms, the anode efficiency appears not to be a function of the Hall thruster channel dimensions:

$$\eta_a \propto \alpha \theta_d^2 \frac{\gamma^2}{\gamma'} \frac{U_d - \Delta}{U_d} \neq f(h, d, L). \quad (41)$$

Finally, it is worth noticing that for a Hall thruster, the thrust-to-power ratio is not linked to the sizes; it solely depends upon the applied voltage (this is also true for a gridded ion engine³). Voltage losses are always low in comparison with the applied voltage, $\Delta \ll U_d$, hence the thrust per unit input power is:

$$\frac{T}{P} \propto \frac{1}{\sqrt{U_d}} \propto \frac{1}{I_{sp}}. \quad (42)$$

This last equation shows that for a given input power, increasing the specific impulse reduces the thrust that can be produced.

These relations between the performances and the dimensions are in agreement with those described by Daren et al.^{3,10}. If one considers, like they do, a constant number density n_n , a constant discharge voltage U_d and a geometric similarity such as $R \propto r$, it appears that the thrust, the electrical power and the discharge current vary as the square of the channel mean diameter.

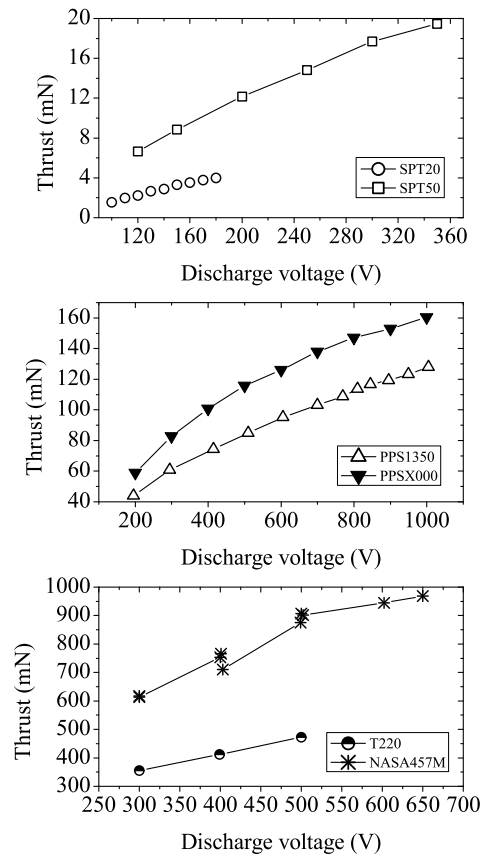


Fig. 2: Thrust as a function of the applied discharge voltage for various Hall effect thrusters: SPT20 (0.47 mg/s), SPT50 (1.0 mg/s), PPS[®]1350 (3.5 mg/s), PPS[®]X000-ML (5.0 mg/s), T220 (19.4 mg/s) and NASA-457M (35.2 mg/s).

IV. Performance and geometry data

A Description of the database

A thorough open literature search using a wide range of resources combined with data-gathering within the French research program on electric propulsion allowed us to create a large database on Hall effect thrusters performances. The database contains information about thruster geometry as well as performances, notably the thrust T , the specific impulse I_{sp} and the anode efficiency η_a for a series of 33 different single-stage Hall thrusters. The database also includes information about the magnetic field strength B , the discharge channel wall materials and the propellant gas. The entire database covers a vast range of input power that stretches from 10 W up to 50 kW and a large collection of data points in terms of applied discharge voltage and gas mass flow rate. A broad range of thrust level is certainly covered, going from 0.4 mN with a micro Hall thruster up to almost 3 N delivered by the high-power thruster developed at NASA. In this work, we focus on Hall thrusters equipped with BN-SiO₂ channel walls and operating with xenon as a propellant gas.

B Example of available data

A part of the collected data in terms of thrust level is displayed in Fig. 2 for Hall thrusters having BN-SiO₂ walls and burning xenon. The thrusters used to construct the figure are the following: a laboratory model of the low power SPT20 thruster¹⁸, a SPT50 thruster manufactured by the Kurchatov Institute¹⁸, the 1.5 kW-class PPS[®]1350 HET developed and manufactured by Snecma¹⁶, the 5 kW-class PPS[®]X000-ML thruster which is a laboratory version of the PPS[®]5000 technology demonstrator devel-

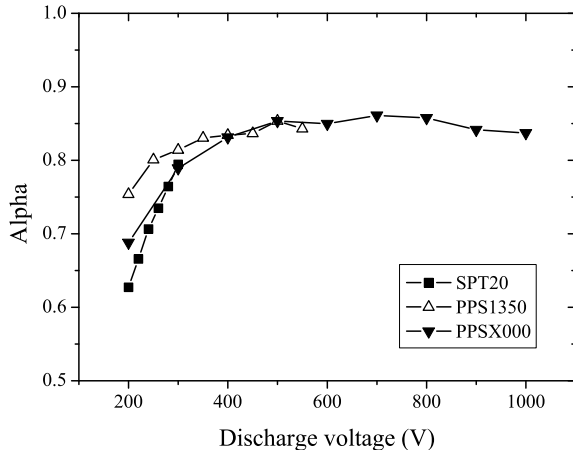


Fig. 3: Propellant conversion efficiency α as a function of the discharge voltage for three types of Hall thrusters running on xenon. The value of α is obtained from thrust measurements, see Eq. (44), assuming that the beam contains mainly singly-charged xenon ions.

oped by Snecma¹⁶, the 10 kW T220 designed and built by TRW and Space Power Inc.¹⁹, as well as the 50 kW-class NASA-457M thruster²⁰. As can be seen in Fig. 2, the thrust of course increases with U_d . When operating at 0.5 mg/s and $U_d = 100$ V, the low-power SPT20 thruster delivers 1.5 mN of thrust. On the opposite side of the thrust domain, the high-power NASA-457M thruster furnishes 970 mN of thrust when running at 35.2 mg/s and $U_d = 650$ V. Information about the specific impulse and the thrust efficiency can be found in other articles^{12,16}.

The propellant conversion efficiency α is the ratio of the ion mass flow rate to the propellant mass flow rate, see Eq. (18):

$$\alpha = \frac{\dot{m}_i}{\dot{m}_n}. \quad (43)$$

The parameter α is not constant for a given thruster geometry, but it depends on the discharge voltage and the mass flow rate. The value of α can be directly inferred from the thrust performance:

$$\alpha = \frac{T}{\dot{m}_n \bar{v}_i} \approx \frac{T}{\dot{m}_n} \sqrt{\frac{m_n}{2e(U_d - \Delta)}}. \quad (44)$$

The right hand side of this equation is valid under the assumption that the extracted beam is mostly composed of singly-charged ions. Figure 3 shows the calculated values of α for three different thrusters as a function of the applied voltage U_d when only Xe^+ ions are taken into account. This figure indicates that α does depend neither on the thruster size nor on the value of U_d as soon as $U_d > 250$ V. Using expressions previously established for T and \dot{m}_n , it appears that the propellant conversion efficiency weakly depends on the geometry and the operating parameters: $\alpha \approx \text{constant}$, in compliance with measurements.

As can be seen in Fig. 3, α increases quickly with the applied voltage, and for $U_d > 250$ V, it approaches a fixed value around 0.85. The growth of α is naturally connected with the electron temperature through the ionization process. The electron temperature is known to increase with the applied voltage²¹. Actually, the production of multiply-charged ions must also be dealt for accurately assessing the value of α ²². According to the collected data set, the calculated values of α vary between 0.3 and 0.96, not taking into account the micro thruster. For low voltages, α drops quickly due to a weak electron temperature. For an input power higher than 1 kW and an applied voltage above 300 V, the quantity α is commonly in the range 0.8-0.9. The curves in Fig. 3 give slightly underestimated values as the voltage losses term Δ was not accounted for. Nevertheless, the value of α obtained when using the ion velocity measured by way of a repulsing potential analyzer in the thruster near field are close to the ones computed with $e \cdot U_d$ as kinetic energy¹². That means the voltage losses are much below U_d and the error associated with α is small.

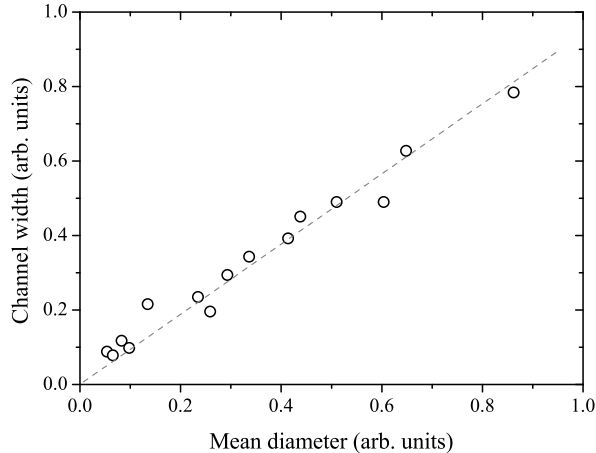


Fig. 4: Channel width h as a function of the channel mean diameter d for a variety of Hall effect thrusters (sizes are in arbitrary units). The two dimensions d and h are proportional.

C Atom density constraint

It was shown in a previous paper that there is an optimum atomic number density n_n in order to keep the physical processes at work in a Hall thrusters unchanged, to warrant a high efficiency and to limit the thermal load as well as the wall wear¹². According to the large amount of gathered data, the critical value that turns out to guarantee a satisfying operation is $n_c = 1.2 \times 10^{19} \text{ m}^{-3}$. This is also the value that is commonly found in literature³. When $n_n < n_{n,c}$, the collision events between atoms and electrons are too scarce to maintain a high ionization level. The ionization mean free path is equal to 0.4 mm for $n_n = n_{n,c}$ (with $T_n = 800 \text{ K}$ and $T_e = 20 \text{ eV}$), much below the channel length and width. For $n_n = 10^{18} \text{ m}^{-3}$, one finds $\lambda_i = 5 \text{ mm}$. The mean free path is then obviously too long. When $n_n > n_{n,c}$, the electron containment due to the magnetic barrier is weakened due to the high electron-atoms collision frequency inside the channel. As the electron diffusion perpendicular to the magnetic field increases, the electric field expands and decreases in strength, the overlap between the ionization and acceleration layers stretches out and the electron back stream through the channel outlet rises. As a consequence, the thruster efficiency drops. For instance, a straightforward calculation indicates that with $n_n = 10^{20} \text{ m}^{-3}$, the ion and electron current magnitudes are identical at the channel exhaust. Details of the calculation can be found in Appendix VIII..

The existence of a critical atom number density $n_{n,c}$ leads to a surprising result. According to Eq. (15), the channel width h must be proportional to the channel mean diameter d : $h \propto d$. This unexpected relation can be verified using the database. In Fig. 4, the channel width is plotted as a function of the mean diameter for different thrusters covering a broad power range (units are arbitrary). As can be seen, the two dimensions h and d are indeed proportional. Therefore, considering an optimum atomic number density n_c , one can refine the scaling laws since only two dimensions remain.

Note that, due to $n_{n,c}$, there is also a critical electron number density to ensure an efficient thruster operation. The ionization degree being roughly 10% in a Hall thruster, the critical electron density lies around 10^{18} m^{-3} .

V. Scaling laws in the case of high assumptions

A List of high simplifying assumptions

In order to simplify the determination of scaling laws from the set of equations previously presented, the following assumptions have been made first:

- all quantities are steady in time,
- the electron temperature is constant and homogeneous whatever the operating conditions,

- the propellant gas has a uniform and fixed temperature all over the channel, hence a constant propellant velocity,
- the potential energy is fully converted into kinetic energy and all ions experience the whole potential drop, of which the magnitude is U_d ($\Delta = 0$),
- plasma-wall interactions are taken into account through heat load to the channel walls,
- the magnetic field is uniform; solely its value at the exit plane is considered,
- electron transport across the magnetic barrier is considered as classical: no anomalous transport is accounted for within the region of strong magnetic field,
- there are no multiply-charged ions in the plasma ($\gamma = \gamma' = 1$),
- a parallel monokinetic ion beam is produced, i.e. the plasma jet divergence is null ($\theta_d = 1$).

B Set of scaling laws

The scaling laws are then obtained from equations derived in the paragraph III using the set of high assumptions. Therefore they read:

$$T = C_{T1} \dot{m} \sqrt{U_d}, \quad (45)$$

$$T = C_{T2} \sqrt{U_d} d^2, \quad (46)$$

$$I_{sp} = C_{I_{sp}} \sqrt{U_d}, \quad (47)$$

$$I_d = C_I d^2, \quad (48)$$

$$P = C_P U_d d^2, \quad (49)$$

$$B = C_{B1}/h d \quad \text{and} \quad B = C_{B2}/L, \quad (50)$$

$$L = C_L \lambda_i, \quad (51)$$

where C factors are proportionality coefficients. The validity of this set of relations can naturally be verified using the database. As an illustration, the figure 5 displays the thrust as a function of the product $\sqrt{U_d} d^2$ for different thrusters. The dashed line represents a linear fit through all data points. For each thruster some values of T are chosen around the point of normal operation.

One should keep in mind that Eqs. (46), (48) and (49) are only valid when n_n is considered to be constant and equal to the critical density $n_{n,c}$. On the contrary, the two relations for the magnetic field strength given by Eq. (50) do not rely on a constant atom number density. As can be verified with Eq. (9), when the atom density is fixed the magnetic field strength B does not depend anymore on the thruster channel diameter d and h . It becomes merely a function of the channel length L . This directly originates from the fact that the electron diffusion perpendicular to the magnetic barrier is assumed to result from electron-atom collision events. Indeed no anomalous electron transport is considered in this study.

C Assessment of proportionality coefficients

In order to assess the required thruster dimensions by way of a scaling method for an available input power or thrust level, it is thus necessary to know the proportionality coefficients C of the aforementioned equations. These coefficients can be determined either empirically, using the database, or analytically as explained in detail in a previous paper¹². However, the empirical approach appears to be more accurate.

The empirically determined proportionality coefficients used for sizing a Hall effect thruster are naturally not given in this contribution as it is sensitive information. Only the C_P and C_T coefficients can be derived from outcomes of this study. Yet, they are available in an article previously published by R. Jankovsky and co-workers²³.

VI. Sizing of high-power Hall thrusters

A Sizing methodology

The scaling process that consists in determining the thruster dimensions L , h and d as well as the magnetic field strength B must be carried out step by step. For a fixed discharge voltage and a given thrust level, the standard procedure is the following:

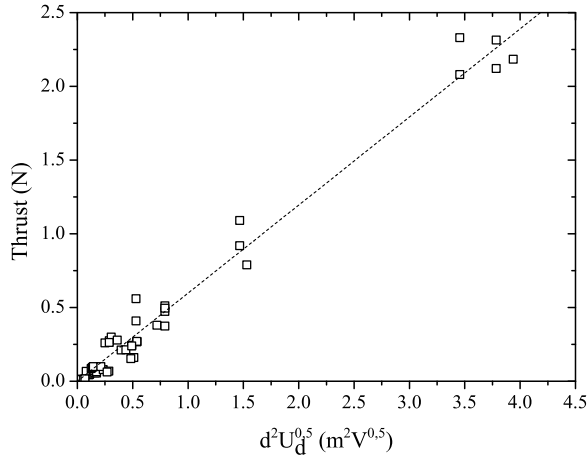


Fig. 5: Thrust as function of $d^2 U_d^{0.5}$ and the linear fit for different Hall effect thrusters (dashed line). For each thruster, some thrust values are chosen around the point of normal operation.

1. The required mass flow rate is determined by means of Eq.(45).
2. The diameter d is obtained using Eq.(46).
3. The discharge current is given by Eq.(48).
4. The electric power reads: $P = I_d U_d$.
5. The size of h is found using the relationship: $h \propto d$.
6. The channel length L is assessed with Eq.(51).
7. The magnetic field strength B is obtained from the relation (50).
8. At least, it should be verified that the number density n_n is close to $1.2 \times 10^{19} \text{ m}^{-3}$.

The channel length is the dimension that is the most difficult to determine as the proportionality coefficient C_L can vary over a broad range of values. As has been shown previously¹², the ratio between λ_i and L is not constant but it can vary considerably for different thruster geometry, gas mass flow rate and discharge voltages. The Melikov-Morozov criterion can however be used to get a first estimate of the channel length by using a mean value for C_L determined from the database.

The procedure for a given input power is slightly different. The channel mean diameter can be determined from the given input power. Knowing the mean diameter d one can then determine the thrust level. The remaining thruster dimensions and operating parameters can then be calculated using the equations presented in paragraph V.

B Thermal load

During thruster operation a certain percentage of the input power P is lost due to the plasma-wall interactions. Indeed, as shown in²⁴, a relatively large energy flux q_p is deposited onto the discharge channel walls, mostly due to ion and electron bombardement, which results in a temperature increase of all thruster components. Naturally, there is a maximum amount of power that can be passed to the walls in order to limit the thermal load and to minimize the sputtering yield of the wall material. One can easily set a maximum wall temperature T_{max} above which an efficient operation of a Hall thruster is not possible. The temperature T_{max} therefore represents a thermal constraint and it must be accounted for when designing a thruster.

A semi-empirical time-dependent thermal model of a Hall effect thruster has been developed in order to determine the energy flux q_p from a measurement of the temporal evolution of the channel wall temperature²⁴. Yet, this model can be used the other way, i.e. to determine the wall temperature from

Dimensions	Parameter	Parameters	Performances
$d = 270 \text{ mm}$	$U_d = 500 \text{ V}$	$P = 17.2 \text{ kW}$	$T = 1 \text{ N}$
$L = 70 \text{ mm}$	$\dot{m} = 41.5 \text{ mg/s}$	$n_n = 1.3 \times 10^{19} \text{ m}^{-3}$	$I_{sp} = 2456 \text{ s}$
	$I_d = 34.3 \text{ A}$	$T_{wall} = 670 \text{ K}$	$\eta = 70 \%$

Table 1: Dimensions, parameters and performances evaluated from scaling laws for a thruster delivering 1 N of thrust

the applied power and the channel size. Here a simplified model of the thruster discharge chamber is used. The thermal enclosure is solely composed of the external and the internal cylindrical walls, meaning that the anode and the rear part of the channel are not taken into account. A more detailed description of the thermal model geometry is given in a previous article¹².

In order to assess the channel wall temperature, only the steady-state wall temperature, i.e. the equilibrium temperature, is of relevance, meaning that the transient regime is ignored. As heat conduction through the channel walls can be neglected, radiation is the only heat transfer mechanism to take into account.

Knowing the thruster dimensions L , h and d , the wall temperatures T_{int} and T_{ext} can be computed as a function of the power transferred to the channel walls by the plasma wall interactions P_{wall} . As it was shown in a previous work²⁴, the ratio $\frac{P_{wall}}{P_{input}}$ is a function of the thruster size and it decreases when the size rises. In short, the trend originates from the fact that the ratio of channel side wall area A_{wall} (\sim loss term) to ion ejection area A_{eject} (\sim thrust generation term) decreases with the size. Indeed, when neglecting losses at the channel back, the ratio $\frac{A_{wall}}{A_{eject}}$ and hence the ratio $\frac{P_{wall}}{P_{input}}$ is equal to $\frac{2L}{h}$. When the Hall thruster operates around the critical atom number density $n_{n,c}$, the channel length L stays roughly unchanged whereas the channel width h increases with the input power P . The process of calculating the wall temperatures can be iterative: in case that the wall temperature is above T_{max} , the dimensions must be changed until the thermal constraint is satisfied.

In this work the maximum temperature for the BN-SiO₂ walls is set to: $T_{max} = 900 \text{ K}$ in compliance with outcomes of a study on the thermal behavior of a Hall thruster performed a few years ago²⁵. Since the value of d and h given by the scaling laws is quite reliable, it appears better to rather modify the channel length L than the mean diameter d or the channel width h , in case that an iterative loop is necessary to satisfy the thermal constraint.

C Design of a 20 kW Hall thruster

High power Hall effect thrusters in the range of 10-30 kW and able to deliver a thrust level around 1 N with a specific impulse of about 2500 s, are thought to be used as primary propulsion system for robotic space probes during interplanetary journeys^{1,26,27}. Such high-power Hall thrusters may also be of interest for orbit transfer maneuvers of large satellites. Only a few high-power prototypes have been developed in the world so far and a significant research effort on this specific technology is now appearing within Europe. For this reason, the sizing method based on the aforementioned widely applicable scaling laws in combination with our large database is employed to design a 20 kW-class thruster with a thrust level of 1 N.

The discharge voltage is fixed to $U_d = 500 \text{ V}$ in order to limit the thermal charge and the secondary electron emission. Xenon is used as propellant gas. The thruster channel walls are assumed to be made of BN-SiO₂ ceramics. The wall losses for the thermal constraint are fixed to 4% of the applied power and the ionization efficiency α is fixed to 0.9.

The dimensions, the parameters and the estimated performances of a 20 kW-class Hall thruster are given in Table 1. The external wall temperature is $T_{ext} = 640 \text{ K}$ and the internal wall temperature is $T_{int} = 700 \text{ K}$.

D Design of a 100 kW Hall thruster

The scaling methodology previously described has also been employed to determine the channel size of a 100 kW Hall thruster. Such a high-power thruster could be used as propulsion device for cargo missions to the Moon or to Mars and for exploration missions towards far-off planets and asteroids^{28,29}. For a discharge voltage $U_d = 500 \text{ V}$, one finds a mean diameter d of 660 mm. The thruster would then be able to deliver a thrust of 5.8 N with a xenon mass flow rate $\dot{m} = 242.2 \text{ mg/s}$ ($I_d = 200 \text{ A}$ and $I_{Hall} = 600 \text{ A}$).

Considering the calculated mass flow rate, 1 ton of xenon is then consumed within 1147 hours, that means 47 days.

With such dimensions and power level, there are several constraints for thruster building and operation. On a technological viewpoint, building and assembling of ceramic rings may be difficult. In like manner, the magnetic circuit architecture must provide the required field over long distances. Heat evacuation is also a critical issue. In order to produce 100 kW, one needs either very large solar panels or a nuclear battery onboard. Finally, another technical aspect to take into account is the size and the pumping capacity of the test facility for test campaigns and experimental investigations of such a large Hall thruster.

VII. Scaling laws with low assumptions

A List of low assumptions

In order to improve the scaling model it is worth reducing the list of high assumptions given in paragraph V. In the remainder of the work the following assumptions are changed compared to the assumptions presented previously:

- the electron temperature is no longer considered to be constant but it becomes a function of the discharge voltage,
- the potential energy is not fully converted into kinetic energy, hence: $\Delta \neq 0$,
- multiply-charged ions are taken into account (γ and $\gamma' \neq 1$),
- the ion beam is no longer considered to be parallel, hence one must account for the divergence angle of the plasma jet ($\theta_d \neq 1$).

B Available data and scaling laws

Former studies showed that the electron temperature is a function of the applied discharge voltage U_d ²¹. Even if experimental data about the electron temperature is quite rare in the literature, we tried to deduce a law on the evolution of T_e as a function of U_d . The electron temperature was measured by a floating movable probe²¹ in hot and cold regimes in the plasma plume of different Hall thrusters. The different thrusters are: a 2 kW laboratory model with two different configurations, a narrow (Raitses narrow) and a wide (Raitses wide) one²¹ and the NASA-173Mv1 with (NASA-173Mv1¹) and without trim coil (NASA-173Mv1²)³⁰. The maximum electron temperature, that is measured in the ionization region, for the different voltages and thrusters is shown in Fig. 6. The evolution of the electron temperature can be assumed to be linear for the different thrusters. A linear fit through all datapoints gives the following law for the evolution of T_e :

$$T_e = 0.123 \times U_d. \quad (52)$$

As can be seen, this linear fit is not quite precise but it is anyhow in good agreement with the common rule-of-thumb that the electron temperature is about one-tenth of the discharge voltage³. Therefore it will be used for the determination of the scaling laws. Note that here one assumes a single electron temperature whereas due to the peculiar properties of the crossed-field discharge of a HET one should take into account two electron temperature components: T_e along the magnetic field lines and T_e perpendicular to the field lines.

The voltage losses in a Hall effect thruster can be calculated from measurements by Laser-Induced Fluorescence (LIF) or by means of a retarding potential analyzer (RPA). Fig.7 shows the evolution of the loss term Δ as a function of the input power. The analysed thrusters are a SPT100 at a mass flow rate of 2.5 mg/s and the PPS[®]X000-ML on the one hand for a voltage series at a constant mass flow rate of 6 mg/s and on the other hand for a mass flow series at a constant discharge voltage of 300 V. As can be seen in Fig. 7, the term of the voltage losses Δ is almost constant for a given thruster size. Therefore it solely depends on the thruster size and the thruster configuration. For the determination of the scaling laws in this work, a constant value of $\Delta = 50 V$ is used.

The plasma plume of a Hall thruster contains a nontrivial amount of energetic, multiply-charged ions. These multiply-charged ions have a higher velocity than singly-charged ions when they are accelerated through the same potential drop, which results in a higher erosion rate due to multiply-charged ions. The production of multiply-charged is a loss mechanism for thrust, efficiency and mass flow utilization.

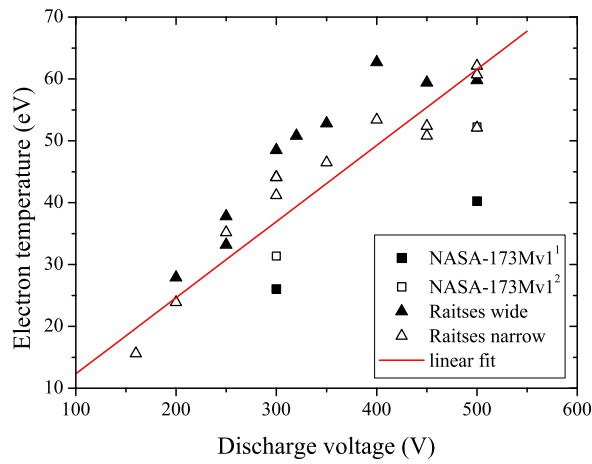


Fig. 6: The maximum electron temperature T_e as a function of the discharge voltage for different Hall thrusters. The equation for the linear fit is: $T_e = 0.123 U_d$.

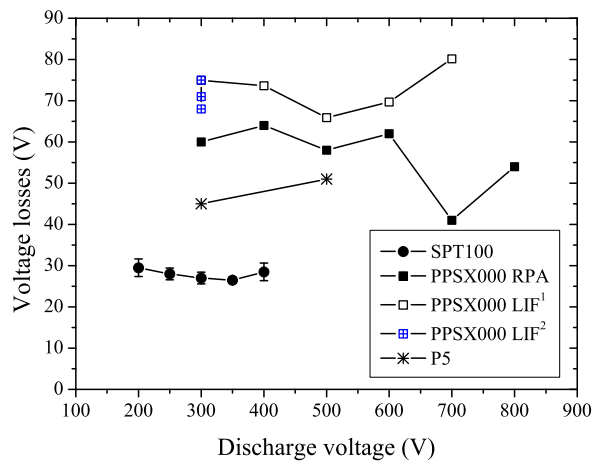


Fig. 7: Voltage losses for the SPT100 and the PPS[®]X000-ML measured by RPA and LIF as a function of the discharge voltage. PPS[®]X000-ML LIF¹ operates at a constant mass flow rate ($\dot{m} = 6 \text{ mg/s}$), whereas PPS[®]X000-ML LIF² operates at a constant discharge voltage ($U_d = 300 \text{ V}$).

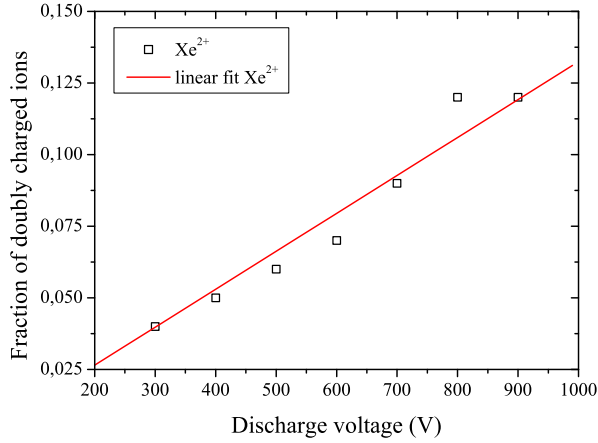


Fig. 8: Fraction of doubly charged ions as a function of the discharge voltage for the NASA-173Mv2 at a mass flow rate of 10 mg/s

Fig. 8 shows the evolution of the fraction of doubly-charged ions Xe^{2+} as a function of the discharge voltage. The ion species fractions were measured in the NASA-173Mv2 plume far-field by means of an E×B probe³¹. The measurements were taken with the thruster operating at an anode mass flow rate of 10.0 mg/s. As can be seen in Fig. 8, the Xe^{2+} species fraction f_{2+} increased from 0.04 to 0.12. The evolution of the Xe^{2+} fraction as a function of the discharge voltage can be approximated by the following linear relation:

$$f_{Xe^{2+}} = 1.325 \times 10^{-4} U_d. \quad (53)$$

The beam divergence angle is set to 30° . Considering an ion beam that diverges uniformly upon the exit of the discharge channel, the beam divergence correction factor is: $\theta_d = \cos(30^\circ) = \frac{\sqrt{3}}{2}$.

The scaling laws in the case of low assumptions can then be obtained from the equations in paragraph III in combination with the list of low assumptions mentioned above and the relations between T_e , Δ and f_{2+} and the discharge voltage U_d .

$$T = C_{T1}^* \gamma \theta_d \dot{m} \sqrt{U_d - \Delta}, \quad (54)$$

$$T = C_{T2}^* \gamma \theta_d \frac{1}{\sqrt{U_d}} \sqrt{U_d - \Delta} \frac{d^2}{L}, \quad (55)$$

$$I_{sp} = C_{I_{sp}}^* \gamma \theta_d \sqrt{U_d - \Delta}, \quad (56)$$

$$I_d = C_I^* \gamma' \frac{1}{\sqrt{U_d}} \frac{d^2}{L}, \quad (57)$$

$$P = C_P^* \gamma' \sqrt{U_d} \frac{d^2}{L}, \quad (58)$$

$$B = C_{B1}^* \frac{\sqrt{U_d}}{h d} \quad \text{and} \quad B = C_{B2}^* \frac{\sqrt{U_d}}{L}, \quad (59)$$

$$L = C_L^* \lambda_i, \quad (60)$$

Again the validity of these relations can be verified using the database. Fig. 9 shows the thrust as a function of the product $\gamma \theta_d \frac{1}{\sqrt{U_d}} \sqrt{U_d - \Delta} \frac{d^2}{L}$ for different thrusters. The dashed line represents a linear fit through all datapoints. As can be seen in Fig. 9 the datapoints for the NASA-457M thruster (asterisk-symbol *) are well above the datapoints for the other thrusters. The reason for this is probably the comparatively long discharge channel. In fact the NASA-457M was designed to be used either with xenon or with krypton. Krypton has a lower mass and a higher ionization energy than xenon, thus the discharge channel must be longer. In this case the channel length of the NASA-457M is a trade-off for the two propellants. As in this work, solely xenon is considered as propellant the NASA-457M is not taken into account for the linear fit.

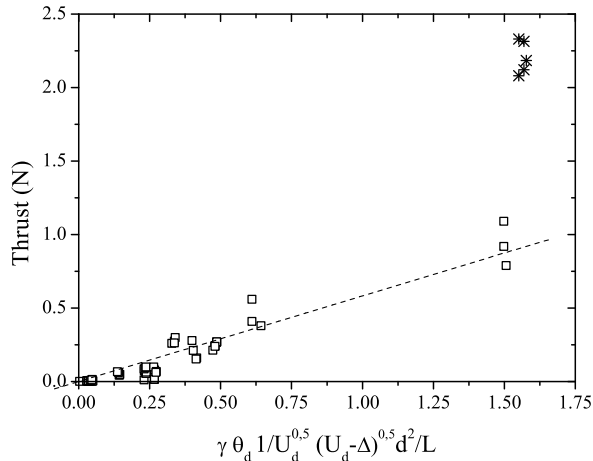


Fig. 9: Thrust as function of $\gamma \theta_d 1/U_d^{0.5} (U_d - \Delta)^{0.5} d^2/L$ and the linear fit for different Hall effect thrusters (dashed line). For each thruster, some thrust values are chosen around the point of normal operation. The NASA-457M thruster is represented by the asterisk-symbol and it is not taken into account for the linear fit.

C Design of two high-power Hall thrusters

The scaling laws developed using the low assumptions are used for the design of the two high-power thrusters in order to be able to compare the outcomes from the two sizing methods and to estimate the impact of the simplifying assumptions. The design-procedure under low assumptions is slightly different. For a fixed discharge voltage of $U_d = 500 V$ and a given thrust level, the product $\frac{d^2}{L}$ can be determined using Eq.(55). The mass flow rate, the specific impulse and the discharge current can be determined using the equations given above (54, 56, 57). Assuming an atomic number density of $n_n = 1.2 \times 10^{19} m^{-3}$ the channel mean diameter can then be calculated from the mass flow rate.

C.1 20 kW Hall thruster

A 20 kW-class Hall thruster able to deliver a thrust of 1 N is designed using the scaling laws under low assumptions. The dimensions, the operating parameters and the performances are presented in Table 2. The external wall temperature is $T_{ext} = 670 K$ and the internal wall temperature is $T_{int} = 745 K$.

C.2 100 kW Hall thruster

For a 100 kW-class thruster the scaling laws under low assumptions give a mean diameter of $d = 723 mm$. This thruster is able to deliver a thrust of $T = 4.97 N$ with a xenon mass flow rate of $\dot{m} = 244.6 mg/s$ and a discharge current of $I_d = 168 A$.

C.3 Comparison

If one compares the results for the two sets of scaling laws, one can deduce that there is no significant difference for the determined operating conditions but for the specific impulse due to the fact that

Dimensions	Parameter	Parameters	Performances
$d = 324 mm$	$U_d = 500 V$	$P = 16.8 kW$	$T = 1 N$
$L = 51 mm$	$\dot{m} = 49.19 mg/s$	$n_n = 1.2 \times 10^{19} m^{-3}$	$I_{sp} = 2072 s$
	$I_d = 33.65 A$	$T_{wall} = 707.5 K$	$\eta = 61 \%$

Table 2: Dimensions, parameters and performances evaluated from scaling laws under low assumptions for a thruster delivering 1 N of thrust

voltage losses Δ are taken into account. Solely the characteristic dimension are bigger in the case of high assumptions.

The accuracy of the scaling laws in the case of low assumptions is however lower than in the case of high assumption as can be seen in Fig. 5 and Fig. 9. One reason for this is the error introduced due to the lack of a sufficiently large number of experimental data. This is especially true for the relation between the electron temperature and the discharge voltage.

In order to get a first estimation of the characteristic dimensions and the operating conditions for a given input power or a given thrust level, the scaling laws developed in the case of high assumptions are definitely sufficient.

VIII. Conclusion

The presented Hall effect thruster sizing method considers the three characteristic thruster dimensions L , d and h , as well as the magnetic field strength B . The method relies on analytical laws that are established from the fundamental principles that govern the physics of a Hall thruster in the frame of simplifying assumptions. Besides, the approach must fulfill stringent rules about atomic number density and channel wall temperature. A vast database that encompasses 33 single-stage Hall thrusters covering a power range between 10 W and 50 kW allows to check the validity of the developed scaling laws and to determine the values of the corresponding proportionality coefficients necessary to dimension a new thruster. In this work two different sets of scaling laws are presented, one in the case of high assumptions and the other in case of low assumptions. Both set of scaling laws are employed to obtain a first estimate of the characteristic dimensions, the operating parameters and the performances of a 20 kW and a 100 kW-class Hall thruster. A comparison of the two methods reveals that reducing the number of assumptions does not lead to an improvement of the accuracy of the scaling laws because of the lack of sufficient experimental data. Therefore the scaling laws under high assumptions are satisfactory to get a first estimate of the geometry and the operating conditions of a thruster, which permits to save time during the design and optimization process.

Acknowledgments

This work is carried out in the frame of the CNRS/CNES/SNECMA/Universités joint research program 3161 entitled “*Propulsion par plasma dans l’espace*”. It is also part of the HiPER collaborative project financially supported in the frame of the 7th European Framework Program under the grant number 218859.

References

- ¹ Frisbee R.H., “Advanced Space Propulsion for the 21st Century”, *J. Propulsion Power*, Vol. 19, No. 6, 2003, pp. 1129-1154.
- ² Zhurin V.V., Kaufmann H.R., Robinson R.S., “Physics of Closed Drift Thrusters”, *Plasma Sources Sci. Technol.* Vol. 8, 1999, pp. R1-R2.
- ³ D. M. Goebel, I. Katz, *Fundamentals of Electric Propulsion*, Wiley, Hoboken, NJ, 2008.
- ⁴ C.R. Koppel, F. Marchandise, M. Prioul, D. Estublier, F. Darnon, “The SMART-1 Electric Propulsion Subsystem Around the Moon: In Flight Experience”, *Proceedings of the 41th Joint Propulsion Conference*, Tucson, Arizona, AIAA paper 05-3671, 2005.
- ⁵ A.I. Morozov and V.V. Savelyev, *Fundamentals of Stationary Plasma Thruster Theory*, Reviews of Plasma Physics **21** (edited by B.B. Kadomtsev and V.D. Shafranov) Consultant Bureau, New York (2000).
- ⁶ V. Kim, “Main Physical Features and Processes Determining the Performance of Stationary Plasma Thrusters”, *J. Propul. Power*, Vol. 14, No. 5, 1998, pp. 736-743.
- ⁷ V. Kim, V. Kozlov, A. Skrylnikov et al., “Development and Investigation of the SPT-20 and SPT-25 Laboratory Models”, *Proceedings of the 1st Annual International Conference and Exhibition. Small*

Satellites: New technologies, achievements, problems and prospects for the International co-operation in the new millenium, section VIII "Jet Propulsion", Moscow, 2000.

- ⁸ J. Ashkenazy, Y. Raitses, G. Appelbaum, "Low Power Scaling of Hall Thrusters", *Proceedings of the 2nd European Spacecraft Propulsion Conference*, Noordwijk, The Netherlands, ESA Publications Division, 1997.
- ⁹ V. Khayms, M. Martinez-Sanchez, "Design of Miniaturized Hall Thruster for Microsatellites", *Proceedings of the 32nd Joint Propulsion Conference*, Lake Buena Vista, AIAA paper 96-3291, 1996.
- ¹⁰ Y. Daren, D. Yongjie, Z. Zhi. "Improvement on the Scaling Theory of the Stationary Plasma Thruster", *J. Propulsion Power*, Vol. 21, No. 1, 2005, pp. 139-143.
- ¹¹ T. Misuri, F. Battista, C. Barbieri, E.A. De Marco, M. Andrenucci, "High Power Hall Thruster Design Options", *Proceedings of the 30th International Electric Propulsion Conference*, Florence, Italy, IEPC paper 07-311, 2007.
- ¹² K. Dannenmayer, S. Mazouffre, "Sizing of Hall Effect Thrusters with Input Power and Thrust Level: An Empirical Approach", *J. Tech. Phys.* Vol. 49, No. 3-4, pp. 231-254, 2008.
- ¹³ M. A. Lieberman, A. J. Lichtenberg, *Principles of Plasma Discharges and Materials Processing*, John Wiley & Sons, Inc., New York, 1994
- ¹⁴ J.W. Koo, I.D. Boyd, "Modelling of Anomalous Electron Mobility in Hall Thrusters", *Phys. Plasmas*, Vol. 13, 2006 and references herein.
- ¹⁵ J.D. Huba, *NRL Plasma Formulary*, Naval Research Laboratory, Washington, 2007.
- ¹⁶ S. Mazouffre, A. Lazurenko, P. Lasgorceix, M. Dudeck, S. d'Escrivan, O. Duchemin, "Expanding Frontiers: Towards High Power Hall Effect Thrusters for Interplanetary Journeys", *Proceedings of the 7th International Symposium on Launcher Technologies*, Paper O-25, 2007.
- ¹⁷ A. Gallimore, "Near- and Far-Field Characterization of Stationary Plasma Thruster plumes", *J. Spacecraft Rockets*, Vol. 38, No. 3, 2001, pp. 441-453.
- ¹⁸ G. Guerrini, C. Michaut, M. Dudeck, M. Bacal, "Parameter Analysis of Three Small Ion Thrusters", *Proceedings of the 2nd European Spacecraft Propulsion Conference*, Noordwijk, The Netherlands, ESA Publications Division, 1997.
- ¹⁹ R.S. Jankovsky, C. McLean, J. McVey, "Preliminary Evaluation of a 10kW Hall Thruster", *Proceedings of the 37th AIAA Aerospace Science Meeting and Exhibit*, Reno, Nevada, AIAA paper 99-0456, 1999.
- ²⁰ D.H. Manzella, R.S. Jankovsky, R.R. Hofer, "Laboratory Model 50kW Hall Thruster", *Proceedings of the 39th Joint Propulsion Conference*, Indianapolis, Indiana, AIAA paper 02-3676, 2002.
- ²¹ Y. Raitses, D. Staack, M. Keidar, N.J. Fisch, "Electron-Wall Interaction in Hall Thrusters", *Phys. Plasmas*, Vol. 12, 2005, pp. 057104-1,057104-9.
- ²² A. Lazurenko, V. Vial, A. Bouchoule, A. Skrylnikov, V. Kozlov, V. Kim, "Dual-Mode Operation of Stationary Plasma Thrusters", *J. Propul. Power*, Vol. 22, No. 1, 2006, pp. 38-47.
- ²³ R.S. Jankovsky, S. Tverdokhlebov, D. Manzella, "High Power Hall Thruster", *Proceedings of the 35th Joint Propulsion Conference*, Los Angeles, CA, AIAA-paper 99-2949, 1999.
- ²⁴ S. Mazouffre, K. Dannenmayer, J. Pérez-Luna, "Examination of Plasma-Wall Interactions in Hall Effect Thrusters by Means of Calibrated Thermal Imaging", *J. Appl. Phys.*, Vol. 102, No. 2, 2007, pp. 023304-1, 023304-10. 23304, 2007
- ²⁵ S. Mazouffre, P. Echegut, M. Dudeck, "A Calibrated Infrared Imaging Study on the Steady State Thermal Behavior of Hall Effect Thrusters", *Plasma Sources Sci. Technol.*, Vol. 15, 2006, pp. 13-22.
- ²⁶ K.E. Witzberger, D. Manzella, "Performances of Solar Electric Powered Deep Space Missions Using Hall Thruster Propulsion", *Proceedings of the 41st Joint Propulsion Conference*, Tucson, Arizona, AIAA paper 05-4268, 2005.

- ²⁷ L. Johnson, R. A. Meyer, K. Frame, “In-Space Propulsion Technologies for Robotic Exploration of the Solar System”, *Proceedings of the 42nd Joint Propulsion Conference*, Sacramento, CA, AIAA paper 06-4687, 2006.
- ²⁸ R. Spores, J. Monheiser, B.P. Dempsey, D.Wade, K.Creel, D.Jacobson, G.Drummond, “A Solar Electric Propulsion Cargo Vehicule to Support NASA Lunar Exploration Progammm”, *Proceedings of the 29th International Electric Propulsion Conference*, Princeton, New Jersey, IEPC paper 05-320, 2005.
- ²⁹ T.M. Randolph, R.C. Dougherty, S.R. Oleson, D.I. Fiehler, N. Dipprey, “The Prometheus 1 Spacecraft Preliminary Electric Propulsion System Design”, *41st Joint Propulsion Conference*, Tuscon, Arizona, AIAA paper 05-3889, 2005.
- ³⁰ J.A. Linnel, A.D. Gallimore, “Internal Plasma Potential Measurement of a Hall Thruster Using Plasma Lens Focusing”, *Physics of Plasma*, Vol. 13, 2006, pp. 103504-1, 103504-9.
- ³¹ R.R. Hofer, A.D. Gallimore, “Ion Species Fractions in the Far-Field Plume of a High-Specific Impulse Hall Thruster”, *39th Joint Propulsion Conference*, Huntsville, Alabama, AIAA paper 03-5001, 2003.

Appendix Upper limit for the atom number density

As has been explained in paragraph IV there is a critical atom number density. One possibility to calculate an upper limit for this critical atom number density is to assume that the electron current magnitude matches the ion current magnitude at the thruster channel exhaust due to numerous electron-atom collisionary events. In that case ($j_i = j_e$) the efficiency of a Hall thruster is very low. The current densities read:

$$e n_e \mu_e E = e n_e v_i, \quad (61)$$

where μ_e is the electron mobility. Here we solely consider the perpendicular electron mobility:

$$\mu_{e\perp} = \frac{m_e \nu_{en}}{e B^2} \quad \text{with} \quad \nu_{en} = n_n \sigma_{en} v_e. \quad (62)$$

Therefore the atom number density reads:

$$n_n = \frac{e B^2}{m_e \sigma_{en} v_e E} \sqrt{\frac{e U_d}{m_i}}. \quad (63)$$

For a magnetic field strength $B = 150 \text{ G}$, a discharge voltage $U_d = 300 \text{ V}$ and an electric field strength $E = 300 \frac{\text{V}}{\text{cm}}$, one finds an upper limit for the atom number density $n_{n,c} = 1.5 \times 10^{20} \text{ m}^{-3}$.